Numerical analysis of the optimized performance of the electron cyclotron wave system in a HL-2M tokamak*

Jing-Chun Li(李景春)[1], Xue-Yu Gong(龚学余)[1,†], Jia-Qi Dong(董家齐)[2], Jun Wang(王俊)[2], and Lan Yin(尹岚)[3]

[1] School of Nuclear Science and Technology, University of South China, Hengyang 421001, China
[2] Southwestern Institute of Physics, P O Box 432, Chengdu 610041, China
[3] School of Mathematics and Physics, University of South China, Hengyang 421001, China

(Received 3 June 2015; revised manuscript received 30 November 2015; published online 20 February 2016)

The capabilities of current drive, neoclassical tearing mode (NTM) stabilization, and sawtooth control are analyzed for the electron–cyclotron wave (ECW) system in a HL-2M tokamak. Better performance of the upper launcher is demonstrated in comparison with that of a dropped upper launcher, in terms of J_{EC}/J_{bs} for NTM stabilization and $I_{ECCD}/(\Delta\rho_{tor})^2$ for sawtooth control. 1-MW ECW power is enough for the 3/2 NTM stabilization, and 1.8-MW ECW power is required to suppress 2/1 NTM in a single null divertor equilibrium with 1.2-MA toroidal current with the upper launcher. Optimization simulation of electron–cyclotron current drive (ECCD) is carried out for three mirrors in an equatorial port, indicating that the middle mirror has a good performance compared with the top and bottom mirrors. The results for balanced co- and counter-ECCD in an equatorial port are also presented.

Keywords: HL-2M, electron–cyclotron current drive, neoclassical tearing modes, sawtooth

PACS: 52.35.Hr, 52.55.Fa, 52.55.Wq, 52.35.Py **DOI:** 10.1088/1674-1056/25/4/045201

1. Introduction

Electron–cyclotron current drive (ECCD) has become a widely used way to drive current and stabilize magnetohydrodynamic (MHD) instabilities in toroidal magnetic confinement devices, since the electron–cyclotron (EC)-driven current profiles are spatially localized and the EC current drive efficiency is competitive with other approaches, such as neutral beam.[1–4] The HL-2M project is the up-grade of the HL-2A tokamak with plasma elongation up to 1.8. The goal of the HL-2M is to illuminate important research issues such as the physics of plasma confinement, transport, high energy particles, MHD stability, and the interaction between the first wall and plasma for fusion study.[5] On one hand, the HL-2M tokamak will largely take advantage of many systems of the present HL-2A, while, on the other hand, the HL-2M will have many advantages in systems of heating, current drive, diagnostics, power suppliers, etc.,[6,7] in comparison with the HL-2A.

The 1-MW electron–cyclotron wave on the HL-2M will be injected to the plasma through the single beam antenna in a Φ200-mm upper launcher (UL) port. A new 1×2 multiple beam antenna with 2-MW input power in a Φ300-mm dropped upper launcher (DUL) port, which is lowered by approximately 10 cm from the UL, is also planned. In addition, the antenna is 3×3 multiple beam and the total input power is 6 MW, composed of 6 gyrotrons of 0.5 MW each and 3 gyrotrons of 1 MW each in the equatorial port. The frequency for the electron–cyclotron wave (ECW) system to be built is 140 GHz. At 140 GHz, EC waves are injected as an X-mode and are absorbed mainly at the second harmonic, causing the density limit to be twice that of the fundamental O-mode. The functions of the two launchers are different. The equatorial launcher (EL) is good for core heating and current profile control since it induces high driven current of broad density profiles J_{EC}, while the upper launcher is good for MHD instability control since it drives well localized current.[8] However, in order to achieve all the goals mentioned above, detailed calculations should be carried out so as to analyze the system capacity and propose an optimized construction plan before the installation of the ECW system on the HL-2M.

The function of MHD instability control is assigned to the UL. MHD instabilities, prominently the neoclassical tearing mode (NTM) and sawtooth (ST), are of significance for plasma confinement. Considering that the essence of NTM control by ECCD is a supplement of the bootstrap current loss, $\eta_{NTM} = J_{EC}/J_{bs}$ is used as a figure of merit for NTM stabilization.[9] Here, J_{bs} and J_{EC} are the bootstrap and ECCD current densities at the resonant magnetic surface, respectively. For simplicity, we use the following criterion, according to the work by Perkins and Harvey,[9] to estimate the performance with η_{NTM}: the complete NTM suppression is not

*Project supported by the National Natural Science Foundation of China (Grant Nos. 11375085, 11405082, 11505092，11475083, and 11375053), the National Magnetic Confinement Fusion Science Program of China (Grant Nos. 2013GB104004, 2013GB111000, 2014GB107000, and 2014GB108002), and the Natural Science Foundation of Hunan Province, China (Grant No. 2015JJ4044).

†Corresponding author. E-mail: gongxueyu@126.com

© 2016 Chinese Physical Society and IOP Publishing Ltd

likely when $\eta_{\rm NTM} < 1.0$; the complete NTM suppression may be achieved when $\eta_{\rm NTM} < 1.2$; the complete NTM suppression is highly likely when $\eta_{\rm NTM} > 1.2$.

The latest study also indicates that the performances for both NTM stabilization and ST control with different launchers are not the same.[10–12] Thus, it is necessary to identify launchers which have better performances in HL-2M. Two launchers, namely the UL and DUL, are also considered in our simulation. ST activity is another MHD instability that is closely related to plasma performance.[13] Both experimental and theoretical results demonstrate that the localized co-CD just inside (or counter-CD just outside) the $q = 1$ surface may shorten ST free periods.[14] The effectiveness of ST control lies on the modification of magnetic shear inside the $q = 1$ surface. Here, the quantity $\eta_{\rm s} = I_{\rm ECCD}/(\Delta\rho_{\rm tor})^2$ is used to evaluate the performance of ST destabilization,[15] where $\rho_{\rm tor} = \sqrt{\phi/\phi_{\rm max}}$ is the square root of normalized toroidal, flux with $\phi_{\rm max}$ being the toroidal flux enclosed in the last closed flux surface, $I_{\rm ECCD}$ and $\Delta\rho_{\rm tor}$ are the total driven current and its normalized e-fold width, respectively.

The main objectives of the equatorial launcher are to get higher driven current for achieving more localized density profiles efficiently with ECW.[16] Moreover, the recent experiments show that balanced co- and counter-ECCD may achieve 'pure' heating with equatorial launchers.[17] Here, with the HL-2M configuration, we will take a series of optimization calculations and hence obtain the optimized parameters and the conditions for pure heating, and the corresponding driven current profiles as well.

The rest of this paper is organized as follows. The TORAY code is introduced and the parameters of HL-2M are presented in Section 2. We report the efficiencies for NTM stabilization and ST control with the UL and the DUL, and a performance comparison between UL and DUL in Section 3. The capabilities of the EL are presented and the results of central co- and counter-ECCD are given in Section 4. Brief conclusions are given in Section 5.

2. TORAY code and the parameters of HL-2M

The TORAY ray tracing code was developed at General Atomics and is primarily aimed at calculating the ECW trajectory, deposition, and current drive.[18–21] Its main characteristics are easy to read, efficient, and highly modulized. So far, TORAY has been commonly benchmarked with other linear, quasi-linear,[22,23] Gaussian beam codes, and quasi-optical codes. Here, thirty rays with a Gaussian distribution in the TORAY code were chosen to launch under different conditions, and the Lin-Liu model[24] was chosen to calculate the current drive efficiency. The beam width here is 2 cm. For TORAY, the poloidal injection angle α is the counter-clockwise angle measured from the up vertical direction. The toroidal injection angle β is the counter-clockwise angle measured from the direction of the major radius on the equatorial plane at the launch point.[25]

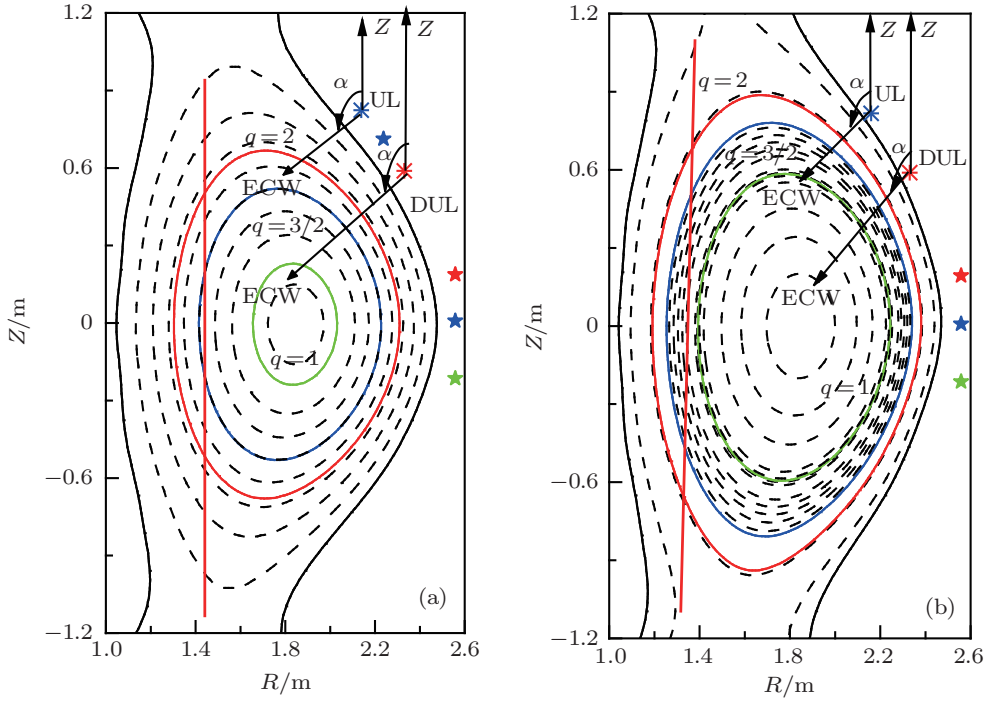


Fig. 1. (color online) (a) HL-2M scenario SD1, with $I_{\rm p} = 1.2$ MA, the three solid contours are the flux surfaces of $q = 2$, $q = 3/2$, and $q = 1$. The two asterisks indicate the locations of the upper (UL, $R = 2.1$ m, $Z = 0.75$ m) and the down upper (DUL, $R = 2.3$ m, $Z = 0.55$ m) launchers, respectively. The three pentagrams represent the locations of the top ($R = 2.52$ m, $Z = 0.2$ m), middle ($R = 2.52$ m, $Z = 0.0$), and bottom ($R = 2.52$ m, $Z = -0.2$) midplane launchers, respectively. (b) Scenario SD2, with $I_{\rm p} = 2.0$ MA, the other parameters are the same as those for panel (a). The poloidal injection angle α and the resonance curves are marked in both panels.

Table 1. Parameters of the HL-2M reference scenarios.

Scenario	I_p/MA	$n_{ec}/(10^{19}/m^3)$	T_{ec}/keV	$\rho_{tor2/1}$	$J_{bs}(\rho_{2/1})/(MA/m^2)$	$\rho_{tor3/2}$	$J_{bs}(\rho_{3/2})/(MA/m^2)$
SD1	1.2	6.0	4.0	0.714	0.164	0.566	0.120
SD2	2.0	6.0	4.0	0.911	0.231	0.814	0.134

The parameters of the HL-2M tokamak are as follows:[26] major radius $R = 1.78$ m, minor radius $a = 0.65$ m, elongation $\kappa = 1.87$, triangularity $\delta = 0.45$, plasma current $I_P = 1.0$ & 2.0 MA, and the magnetic field at magnetic axis $B_t = 1.82$ T for SD1 and $B_t = 2.0$ T for SD2. The scenarios of the two single-null diverted HL-2M equilibria, shown in Fig. 1, were constructed with the EFIT code.[27] The density and temperature profiles are expressed with the empirical formula as follows:

$$n_e = (n_{ec} - n_{ea})[1 - (r/a)^i]^s + n_{ea},$$
$$T_e = (T_{ec} - T_{ea})[1 - (r/a)^i]^s + T_{ea},$$

where n_{ec} and n_{ea} are the core and edge electron densities, respectively, T_{ec} and T_{ea} are the core and edge electron temperatures, respectively, the $i = 1$ and $s = 1/3$ are the empirical indexes,[12] $Z_{eff} = 2.5$ with a flat profile is assumed. The main parameters of the two scenarios are summarized in Table 1, with the bootstrap current density calculated with the transport code ONETWO.[28]

3. Comparison between and analysis of the UL and DUL performances

In order to realize heating and current drive at the plasma edge, and real time control of MHD instability with ECW, an ECRH upper port launcher will be built on the HL-2M. In this launcher, a beam switch will be equipped in the transmission line system. As a result, if we want to control MHD instabilities with ECW, then the upper antenna can be used; if our aims are to implement the central heating and current drive, the equatorial antenna should be switched on. As mentioned before, there are two plans for the upper antenna, i.e., the UL and DUL. For the HL-2M, both launchers cover almost the whole plasma cross section. We will compare the performances of the two launchers in terms of the figures of merit for their main physics objectives in the following.

The ECCD calculations with the TORAY code are carried out for both the UL and DUL launchers. It is generally true that the figures of merit $I_{ECCD}/(\Delta\rho_{tor})^2$ have their maximum values around the same toroidal launch angle for all flux surfaces under consideration in ITER,[11] which is also confirmed in our simulation in the HL-2M tokamak. Thus, we can fix the toroidal launch angle and use the poloidal angle steering only to make a comparison of the performance between UL and DUL launchers. Figures 2 and 3 show the radial deposition position ρ^r_{tor} versus the poloidal angle (Fig. 2(a)), the peak values of the driven current density (with typical current density profiles depicted) versus deposition position (Fig. 2(b)), the normalized e-fold width of the driven current density profile (Fig. 2(c)), and the total driven currents (Fig. 2(d)) for plasma scenarios SD1 and scenario SD2, respectively. The differences in the performance between the two launchers are very clear. From Figs. 2(a) and 3(a), one can see that the radial deposition position moves inward with the increase of the poloidal angle. For SD1, in order to cover the plasma area of interest, the ranges of the poloidal angle larger than 130° and 116° are demanded for the UL and DUL, respectively. For SD2, these poloidal angles should be larger than 110° and 95° for the UL and DUL respectively. Meanwhile, the UL has an outer radial deposition position compared with the DUL when the poloidal angles are the same. This is consistent with what is shown in Fig. 1. The peak values of the driven current density for UL are higher than those for DUL. The total driven currents for UL are almost the same as those for DUL, while the widths of the current density profiles are narrower for the former than for the latter. These figures also demonstrate that the width of the current density profile is nearly independent of the deposition position, i.e., the poloidal angle α, while the profile width for UL is approximately 0.7 of that for DUL. In addition, it is found that the poloidal angle range required to drive a current covering the same radial deposition region is larger for UL than for DUL. For example, the poloidal angle range needed to drive the current from the radial position $\rho^r_{tor} = 0.97$ to $\rho^r_{tor} = 0.61$ is $\Delta\alpha = 38°$ for UL, while $\Delta\alpha = 33°$ is enough for DUL in the case of scenario SD1. This phenomenon is shown more clearly in the case of scenario SD2 where the poloidal angle range needed to drive the current from $\rho^r_{tor} = 0.93$ to $\rho^r_{tor} = 0.53$ is $\Delta\alpha = 36°$, while $\Delta\alpha = 26°$ is required only for DUL.

In order to compare and analyze the efficiencies of NTM stabilization with 1MW ECCD for UL and DUL launchers, we calculate the figures of merit for 2/1 and 3/2 NTM stabilization in the two scenarios. The parameters relevant to the best figure of merit for UL and DUL are shown in Tables 2 and 3, respectively. The results provide the following information about (i) the value of the figure of merit η_{NTM} for NTM control is only larger than 1.2 for the case of 3/2 NTM stabilization in SD1, thus, higher ECW power is needed to stabilize all the NTMs, e.g., 1.8-MW ECW power is needed to suppress 2/1 NTM in SD1 completely with UL. The 2/1 NTM in SD2 is very unstable and its required ECW power reaches as large as 3 MW with DUL; (ii) the value of the figure of merit η_{NTM} for NTM control is higher in scenario SD1 than in scenario SD2 for both launchers; (iii) the value of $I_{ECCD}/(\Delta\rho_{tor})^2$ for UL is a factor of 1.5 higher than that for DUL at $q = 2$ of scenario SD1, and it is a factor of 1.9 higher than that for DUL at the $q = 3/2$ of scenario SD2.

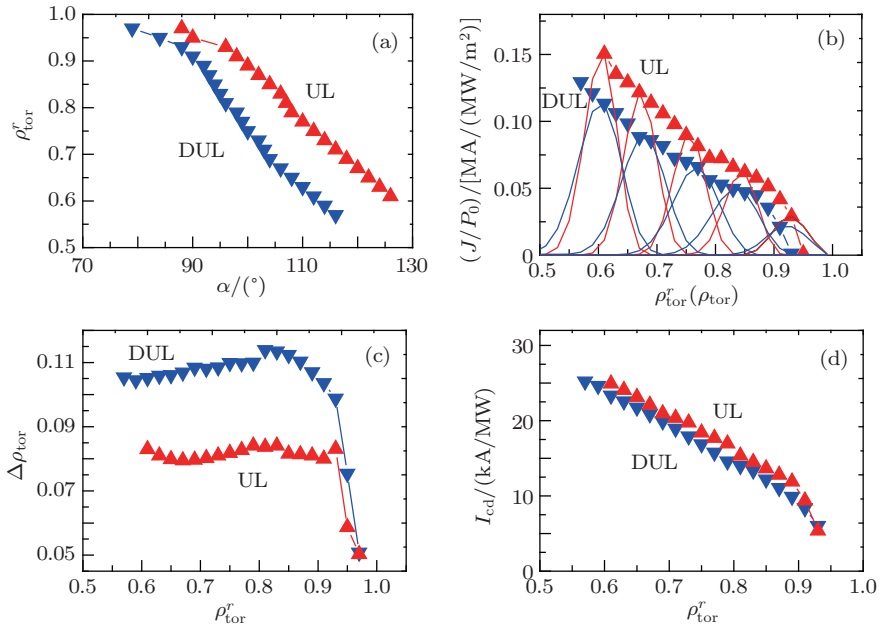


Fig. 2. (color online) Radial deposition position $\rho^r_{\rm tor}$ versus the poloidal angle (a), the peak values of the driven current density (with typical current density profiles depicted) versus $\rho^r_{\rm tor}$ (b), the normalized e-fold width of the driven current density profile versus $\rho^r_{\rm tor}$ (c), and the total driven currents versus $\rho^r_{\rm tor}$ (d) for 1MW of injection power into the scenario SD1 plasma from the DUL and the UL. The toroidal angle $\beta = 204^\circ$.

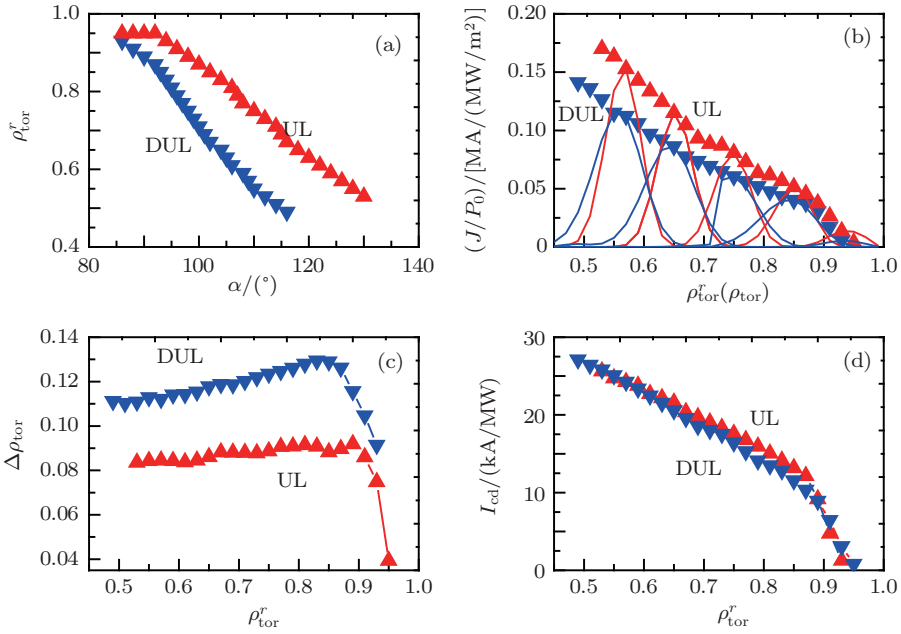


Fig. 3. (color online) The same as Fig. 2, but for the scenario SD2 plasma.

Table 2. Parameters for the best figure of merit for UL with 1-MW ECW injected.

Scenario	q	$\alpha/(^\circ)$	$\beta/(^\circ)$	$J_{\rm EC}/({\rm MA/m^2})$	$I_{\rm ECCD}$/kA	$\Delta\rho_{\rm tor}$	$J_{\rm EC}/J_{\rm b}$	$[I_{\rm ECCD}/(\Delta\rho_{\rm tor})^2]$/MA
SD1	2	118	201	0.110	19.1	0.078	0.67	3.1
SD1	3/2	132	204	0.157	26.1	0.086	1.31	3.5
SD2	2	104	203	0.062	12.5	0.087	0.46	1.7
SD2	3/2	108	202	0.073	14.6	0.084	0.55	2.1

Table 3. Parameters for the best figure of merit for DUL with 1-MW ECW injected.

Scenario	q	$\alpha/(^\circ)$	$\beta/(^\circ)$	$J_{\rm EC}/({\rm MA/m^2})$	$I_{\rm ECCD}$/kA	$\Delta\rho_{\rm tor}$	$J_{\rm EC}/J_{\rm b}$	$[I_{\rm ECCD}/(\Delta\rho_{\rm tor})^2]$/MA
SD1	2	103	200	0.086	18.6	0.097	0.53	2.0
SD1	3/2	123	203	0.124	26.0	0.110	1.03	2.1
SD2	2	96	201	0.054	10.0	0.104	0.40	0.9
SD2	3/2	99	203	0.058	12.3	0.111	0.43	1.0

Concerning the performances of the two launchers for ST control, the most accurate calculations require transport modeling, including a model that incorporates the alpha particles stabilizing effect.[29,30] However, it is feasible to take $\eta_s = I_{ECCD}/(\Delta\rho_{tor})^2$ as a figure of merit to compare the efficiencies of UL and DUL. Figure 4 shows the values of η_s for $P_{EC} = 1$ MW from the UL and DUL in scenarios SD1 and SD2. From this figure, the UL efficiency to control ST in the radial range where $q = 1$ is expected to occur, i.e., $0.3 \leq \rho^r_{tor} \leq 0.6$, could be a factor of ~ 1.6 higher than the DUL efficiency for scenario SD2. There is also a large value of UL efficiency compared with the DUL efficiency in scenario SD1. We conclude that for both NTM stabilization and ST control, better performance could be achieved with UL in the HL-2M tokamak. The possible reason for this may be attributed to the better relation between the geometry of the flux surfaces and the launcher location, causing narrower driven current density profiles and a larger local parallel refractive index $(n_{||})$, thus getting larger values of the driven current in the HL-2M configuration. The better performance for UL here is similar to the TORAY simulations in EAST[12] and is just contrary to the GRAY calculations in ITER.[10] One of the possible reasons is that the calculation in Ref. [10] was performed with a focused and collimated beam, in which however the interference and diffraction effects are important. The systematic analyses of interference and diffraction effects will be performed with other Gaussian beam and quasi-optical codes for the HL-2M and EAST tokamaks in the future.

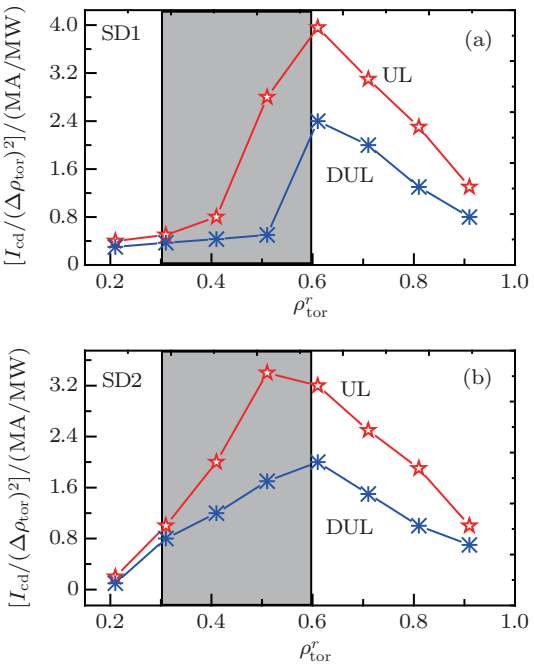


Fig. 4. (color online) Figures of merit η_s for sawtooth control for 1-MW ECW power injected into the plasma of scenario SD1 (a) and SD2 (b) from the UL and DUL. The shaded region indicates the case where the $q = 1$ surface is likely to occur.

From the above results and analyses, we may conclude that for both NTM stabilization and ST control, good performance of the upper launcher is demonstrated in comparison with that of a dropped upper launcher. This consequence comes from the fact that the CD capabilities of UL are better than those of DUL, which can be seen in Ref. [22]. The possible reasons are as follows. The first one is the toroidal effect and the other is that the optical thickness of the resonance is larger when the launch position is higher. More detailed explanations can also be found in Ref. [22].

4. Performances of the equatorial launcher

In order to identify the performances of the EL, ECWs are launched from 3 mirrors, located at $R = 2.52$ m and $z = 0.2$, 0, and -0.2 m, which are called top, middle, and bottom mirrors, respectively. The normalized radius of the peak current density location, the peak current density, the normalized e-folding width of the driven current density profile, and the total driven current versus the toroidal angle are shown in Figs. 5 and 6 for scenarios SD1 and SD2, respectively. The following observations are obtained from these figures: (i) the maximum driven currents of 25 kA/MW and 30 kA/MW are achieved in scenarios SD1 and SD2, respectively; (ii) among the three mirror launchers, the middle mirror launcher has the best performance of current drive, and a maximum value of the peak driven current density, which is about 1.55 times larger than those for the launchers of the top and bottom mirrors; (iii) like the relation between the radial deposition position and the poloidal angle, the larger toroidal angle also makes the ECW power deposit in the inner plasma region. The range of the toroidal angle considered here is large enough for a driven current density at $q = 3/2$; (iv) at a toroidal angle of 204°, the current density profiles are much broader than those obtained with the upper launchers. For instance, in scenario SD2, the width of the current density profile driven from the top mirror launcher is 2 times larger than that from the UL as seen in Figs. 3(c) and 6(c). What should be noticed is that the higher $n_{||}$ makes the ECCD efficiency higher for a large toroidal angle since the electron–cyclotron waves are resonant with electrons of higher parallel velocity. However, a large toroidal angle also has the following limitations: the Doppler effect broadens the current density profile, and the third harmonic absorption appears when the toroidal angle reaches a certain value.[31] An example of this is shown in Fig. 7 for the scenario SD1 with ECW injected at $\beta = 207°$. The third harmonic absorption appears when the toroidal angle is 201° for both the top mirror and the middle mirror, and 204° for the bottom mirror, with a poloidal angle at $\alpha = 90°$ for all the cases. The parasitic third harmonic absorption may play an important role in the scenarios at low magnetic fields. It could strongly reduce the driven current and lead to the X2 mode interaction being

less efficient. However, under some experimental conditions, the injections of X2 and X3 EC waves simultaneously can be used for studying the high power-density EC heating and current drive.[32] The study of the avoidance and utilization of the third harmonic absorption in the HL-2M is an important issue and will be discussed in another paper.

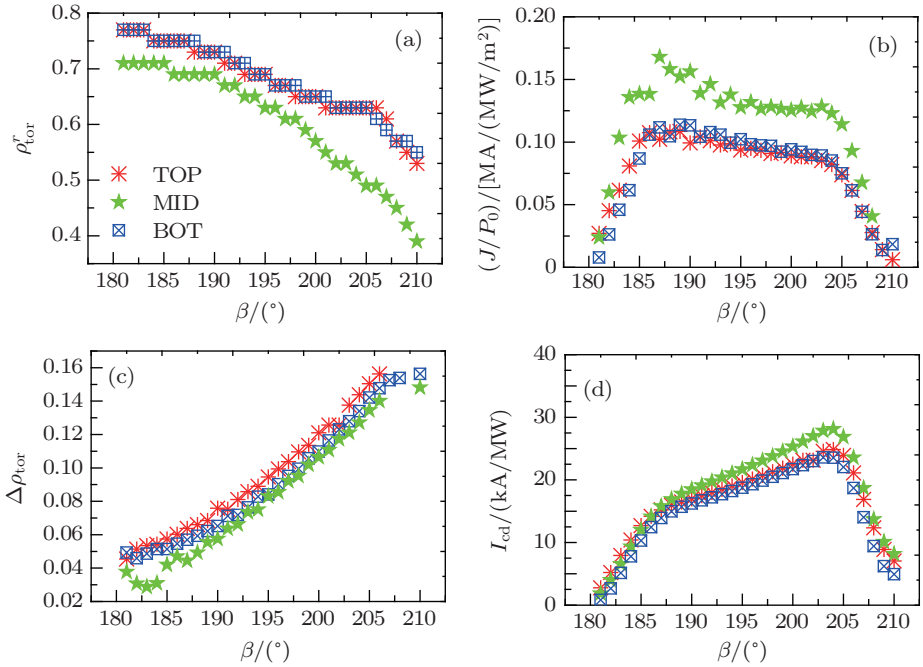


Fig. 5. (color online) Plots of the normalized radius of the peak current density location (a), peak current density (b), the normalized e-folding width of the driven current density profile (c), and total driven current (d), versus toroidal angle for the three mirrors, i.e., the top, middle, and bottom mirrors in the equatorial port. The equilibrium and plasma parameters are those of scenario SD1.

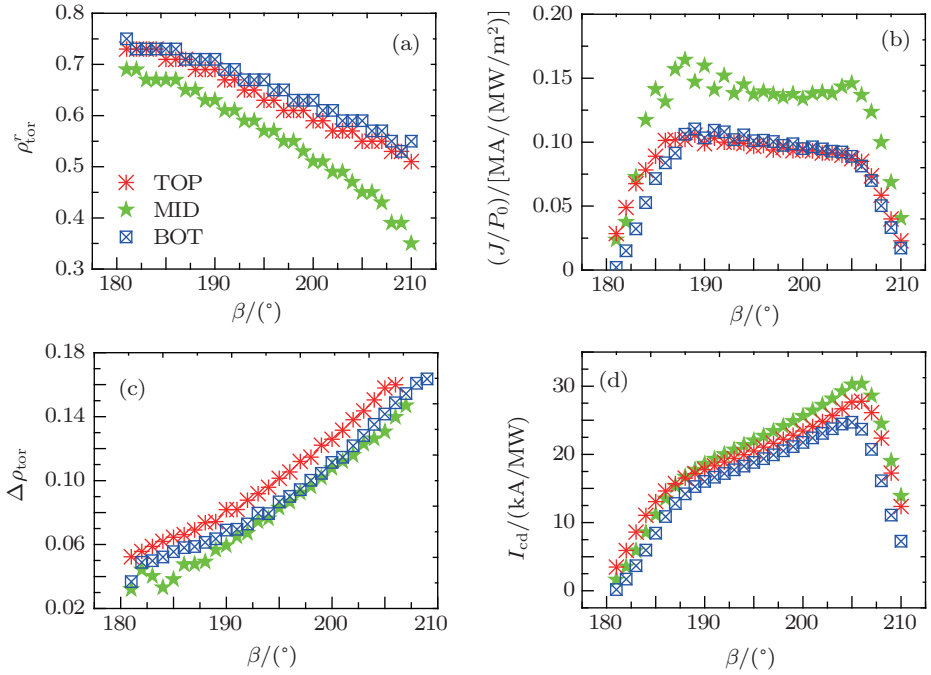


Fig. 6. (color online) The same as Fig. 5, but the equilibrium and plasma parameters are those of scenario SD2.

As mentioned before, the main physics objective for EL is to implement the central plasma heating and current drive. Counter-ECCD (balancing co-ECCD) is required to avoid undesirable peaking of the plasma current profile at the plasma centre.[33] In some cases, it was also employed to demonstrate the possibility of full bootstrap discharge sustainment. By adding counter-ECCD beams to balance the co-ECCD component exactly, the total driven current can be annulled, leaving only the bootstrap component.[34] The current density profiles of co- and counter-ECCD calculated for the two scenarios are shown in Fig. 8. The 1-MW ECW is launched from the top mirror in this case. The total driven currents are

−6.9 kA and +5.8 kA for scenario SD1, and −8.9 kA and +8.8 kA for scenario SD2, both with injection at $\alpha = 100°$ and $\beta = \pm 214°$, where minus and plus signs refer to counter-ECCD and co-ECCD, respectively. The capabilities of co- and counter-ECCD in the HL-2M tokamak would allow a detailed study of ECCD physics.

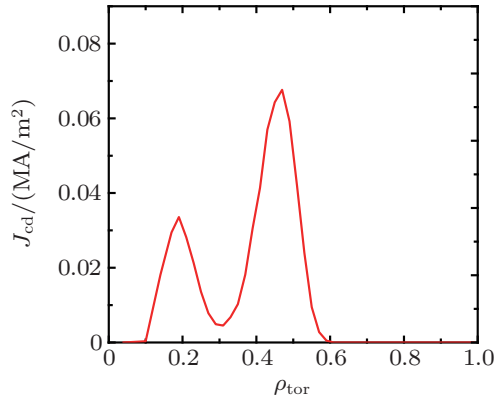


Fig. 7. (color online) Driven current density profile for 1-MW ECW power injected from the middle mirror at $\beta = 207°$ into the plasma of scenario SD1.

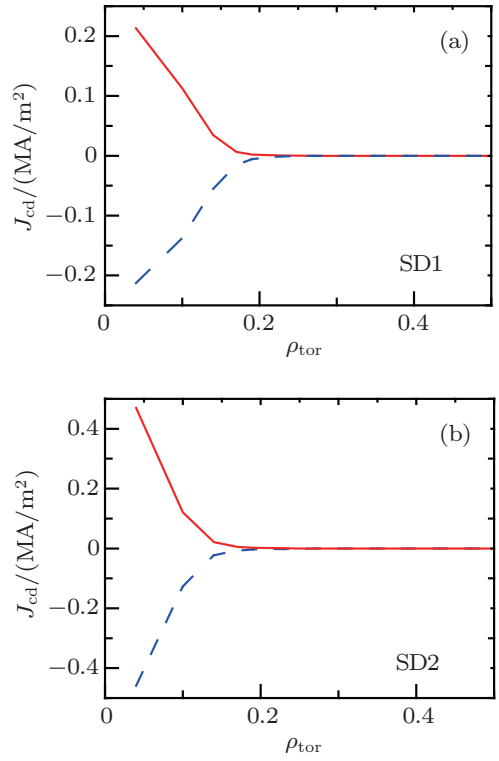


Fig. 8. (color online) Profiles of co-ECCD and counter-ECCD for 1-MW ECW injected from the EL with a poloidal angle $\alpha = 100°$, and toroidal angle $\beta = \pm 214°$ for both scenarios.

5. Conclusions

The capabilities of current drive, NTM stabilization and ST control for the ECW system in the HL-2M are presented using the code TORAY. The performances of the two upper launchers, namely the UL and DUL, are analyzed and compared. For both NTM stabilization and ST control, the UL, by inducing higher driven current density and narrower driven current density profiles, has better performance than the DUL. The values of the figure of merit η_{NTM} for NTM control are shown for 3/2 and 2/1 NTM in both SD1 and SD2, thus the required ECW power for each case of NTM stabilization is clarified. The ECCD characteristics for three mirrors in the equatorial port are also presented, and the following principle results can be drawn. First, for all the launches from the three mirrors, the values of ECCD efficiency have their maxima around the same toroidal launch angle, i.e., 204° for scenario SD1 and 206° for scenario SD2. Second, compared with the top and bottom mirror launchers, the middle mirror launcher has high current drive capabilities and a more localized current density profile. Thus, from a physics point of view, the UL and the middle mirror are highly desirable and should be chosen if the technical solution is acceptable for the HL-2M. Finally, the balanced co- and counter-ECCD in the equatorial port is achieved, demonstrating the feasibility to achieve 'pure' heating with the equatorial port in the HL-2M tokamak. The performance analysis and results in this paper will certainly be useful for optimizing the design and installation of the ECW system in the HL-2M and other tokamak devices, in particular, for suppressing the NTMs and sawteeth.

References

[1] Poli E, Tardini G, Zohm H, Fable E, Farina D, Figini L, Marushchenko N B and Porte L 2013 *Nucl. Fusion* **53** 013011
[2] Gong X Y, Peng X W, Xie A P and Liu W Y 2006 *Acta Phys. Sin.* **55** 1307 (in Chinese)
[3] Chen S Y, Tang C J and Zhang X J 2013 *Chin. Phys. Lett.* **30** 65202
[4] Gong X Y, Shi B R, Zhang J H, Qiu X P and Ling Q 2002 *Acta Phys. Sin.* **51** 2547 (in Chinese)
[5] Xia F, Pan L, Zhao L, Pan W, Song X, Li X Y, Wang C, Lan J T, Chen L Y and Kazuo Nakamura 2012 *Plasma and Fusion Research* **7** 2405048
[6] Li Q 2013 "The Construction Progress of HL-2M Tokamak". In the preceedings of the 25th Symposium on Fusion Engineering (SOFE)
[7] Peng J F, Xuan W M, Wang H B, Li H J, Wang Y Q and Wang S J 2013 *Plasma Sci. Technol.* **15** 300
[8] Henderson M A, Heidinger R, Strauss D, Bertizzolo R, Bruschi A, Chavan R, Ciattaglia E, Cirant S, Collazos A, Danilov I, Dolizy F, Duron J, Farina D, Fischer U, Gantenbein G, Hailfinger G, Kasparek W, Kleefeldt K, Landis J D, Meier A, Moro A, Platania P, Plaum B, Poli E, Ramponi G, Saibene G, Sanchez F, Sauter O, Serikov A, Shidara H, Sozzi C, Spaeh P, Udintsev V S, Zohm H and Zucca C 2008 *Nucl. Fusion* **48** 054013
[9] Perkins F W and Harvey R W 2000 *Bull. Am. Phys. Soc.* **45** 278
[10] Ramponi G, Farina D, Henderson M A, Poli E, Sauter O, Saibene G, Zohm H and Zucca C 2008 *Nucl. Fusion* **48** 054012
[11] Zohm H, Heidinger R, Henderson M, Poli E, Ramponi G, Saibene G and Verhoeven A G A 2005 *J. Phys.: Conf. Ser.* **25** 234
[12] Wang X G, Wu B, Hu Y M, Wang J F, Hu C D and Zhang X D 2012 *Phys. Scr.* **86** 065501
[13] Sauter O, Westerhof E, Mayoral M L, Alper B, Belo P A, Buttery R J, Gondhalekar A, Hellsten T, Hender T C, Howell D F, Johnson T, Lamalle P, Mantsinen M J, Milani F, Nave M F F, Nguyen F, Pecquet A L, Pinches S D, Podda S and Rapp J 2002 *Phys. Rev. Lett.* **88** 105001
[14] Angioni C, Goodman T P, Henderson M A and Sauter O 2003 *Nucl. Fusion* **43** 455
[15] Zohm H, Gantenbein G, Leuterer F, Manini A, Maraschek M, Yu Q and the ASDEX Upgrade Team 2007 *Nucl. Fusion* **47** 228
[16] Prater R 2005 *J. Phys.: Conf. Ser.* **25** 257
[17] Henderson M A, Behn R, Coda S, Condrea I, Duval B P, Goodman T P, Karpushov A, Martin Y, Martynov An, Moret J M, Nikkola P, Porte L, Sauter O, Scarabosio A, Zhuang G and the TCV Team 2004 *Plasma Phys. Control. Fusion* **46** A275
[18] Mazzucato E, Fidone I and Granata G 1987 *Phys. Fluids* **30** 3745

[19] Cohen R H 1987 *Phys. Fluids* **30** 2442

[20] Petty C C, La Haye R J, Luce T C, Humphreys D A, Hyatt A W, Lohr J, Prater R, Strait E J and Wade M R 2004 *Nucl. Fusion* **44** 243-51

[21] Alberti S Goodman T P, Henderson M A, Manini A, Moret J M, Gomez P, Blanchard P, Coda S, Sauter O, Peysson Y and TCV Team 2002 *Nucl. Fusion* **42** 42-5

[22] Li J C, Gong X Y, Dong J Q, Gao Q D, Zhang N and Li F Y 2015 *Phys. Plasmas* **22** 102510

[23] Wang Z T, Long Y X, Dong J Q and He Z X 2013 *Chin. Phys. B* **22** 095201

[24] Lin-Liu Y R, Chan V S and Prater R 2003 *Phys. Plasmas* **10** 4064

[25] Wei W, Ding B J, Zhang X J, Wang X J, Li M H, Kong E H and Zhang L 2014 *Chin. Phys. B* **23** 055201

[26] Cui X W, Pan Y D, Cui Z Y, Li J X, Zhang J H and Mao R 2013 *Plasma Sci. Technol.* **15** 1184

[27] Lao L L, John H St, Stambaugh R D, Kellman A G and Pfeiffer W 1985 *Nucl. Fusion* **25** 1611

[28] Pfeiffer W W, Davidson R H, Miller R L and Waltz R E 1980 "ONETWO: A computer Code for Modeling Plasma Transport in Tokamaks," 1980, General Atomics Report GA-A16178

[29] Merkulov A, Westerhof E, Schuller F C, de Baar M R, Kramer-Flecken A, Liang Y and TEXTOR Team 2004 *Proc. Joint Varenna-Lausanne Int. Workshop on Theory of Fusion Plasmas*, Varenna, Italy, p. 279

[30] Ramponi G, Farina D, A Henderson M, Poli E, Saibene G and Zohm H 2007 *Fusion Sci. Technol.* **52** 193

[31] Li J C, Gong X Y, Dong J Q, Zheng P W, Song S D, Gao Q D and Du D 2015 *Phys. Plasmas* **22** 062512

[32] Gnesin S, Decker J, Coda S, Goodman T P, Peysson Y and Mazon D 2012 *Plasma Phys. Control Fusion* **54** 035002

[33] Farina D, Henderson M, Figini L, Ramponi G and Saibene G 2012 *Nucl. Fusion* **52** 033005

[34] Coda S, Sauter O, Henderson M A and Goodman T P 2008 "Full bootstrap discharge sustainment in steady state in the TCV tokamak", *Proceedings of the* 22*nd IAEA Fusion Energy Conference*, IAEA, 2008 (CRPP-CONF-2008-002): EX/2-3